

Outshining in the Spatially Resolved Analysis of a Strongly-Lensed Galaxy at $z = 6.072$ with *JWST* NIRC*am*

C. Giménez-Arteaga^{1,2}, S. Fujimoto³, F. Valentino^{4,1}, G. B. Brammer^{1,2}, C. A. Mason^{1,2}, F. Rizzo^{1,2}, V. Rusakov^{1,2}, L. Colina⁵, G. Prieto-Lyon^{1,2}, P. A. Oesch^{1,2,6}, D. Espada^{7,8}, K. E. Heintz^{1,2}, K. K. Knudsen⁹, M. Dessauges-Zavadsky⁶, N. Laporte^{10,11}, M. Lee^{1,12}, G. E. Magdis^{1,2,12}, Y. Ono¹³, Y. Ao^{14,15}, M. Ouchi^{13,16,17,18}, K. Kohno^{19,20}, A. M. Koekemoer²¹

We present *JWST*/NIRC*am* observations of a strongly-lensed, sub- L^* , multiply-imaged galaxy at $z = 6.072$, with magnification factors $\mu \geq 20$ across the galaxy. The galaxy has rich *HST*, *MUSE* and *ALMA* ancillary observations across a broad wavelength range. Aiming to quantify the reliability of stellar mass estimates of high redshift galaxies, we perform a spatially-resolved analysis of the physical properties at scales of ~ 200 pc, inferred from SED modelling of 5 *JWST*/NIRC*am* imaging bands covering $0.16 \mu\text{m} < \lambda_{\text{rest}} < 0.63 \mu\text{m}$ on a pixel-by-pixel basis. We find young stars surrounded by extended older stellar populations. By comparing $\text{H}\alpha + [\text{N II}]$ and $[\text{O III}] + \text{H}\beta$ maps inferred from the image analysis with our additional NIRS*pec* IFU data, we find that the spatial distribution and strength of the line maps are in agreement with the IFU measurements. We explore different parametric star formation history forms with *Bagpipes* on the spatially-integrated photometry, finding that a double power-law star formation history retrieves the closest value to the spatially-resolved stellar mass estimate, and other SFH forms suffer from the dominant outshining emission from the youngest stars, thus underestimating the stellar mass – up to ~ 0.5 dex. On the other hand, the DPL cannot match the IFU measured emission lines. Additionally, the ionizing photon production efficiency may be overestimated in a spatially-integrated approach by ~ 0.15 dex, when compared to a spatially-resolved analysis. The agreement with the IFU measurements implies that our pixel-by-pixel results derived from the broadband images are robust, and that the mass discrepancies we find with spatially-integrated estimates are not just an effect of SED-fitting degeneracies or lack of NIRC*am* coverage. Additionally, this agreement points towards the pixel-by-pixel approach as a way to mitigate the general degeneracy between the flux excess from emission lines and underlying continuum, especially when lacking photometric medium-band coverage and/or IFU observations. This study stresses the importance of studying galaxies as the complex systems that they are, resolving their stellar populations when possible, or using more flexible SFH parameterisations. This can aid our understanding of the early stages of galaxy evolution by addressing the challenge of inferring robust stellar masses and ionizing photon production efficiencies of high redshift galaxies.

1. Introduction:

One of the most critical issues in the high-redshift galaxies is inferring robust stellar masses.

Varying the star formation history (SFH), or other assumptions such as the initial mass function (IMF), can have a significant impact in the inferred physical properties.

Spatially-resolved studies:

Sorba & Sawicki (2018): HST data ($z < 2.5$ sample), resolved stellar masses can be up to five times larger than unresolved estimates

JWST \rightarrow Spatially-resolved studies to high redshifts ($z > 2.5$)

Spatially-resolved studies can solve the problem of outshining: young stellar populations dominate the integrated light, hiding underlying older stellar populations (≥ 100 Myr), thus leading to an underestimation of the total mass of the stellar population.

Also, the *JWST* IFU spectra can provide a crucial check on spatially-resolved characteristics derived from modelling the images alone.

2. Data (RXCJ0600-z6-3):

The NIRC*am* observation of a strongly-magnified galaxy at $z = 6.072$ (Fujimoto et al. 2021b; Laporte et al. 2021), observed also with NIRS*pec* IFU. This object behind the massive $z = 0.43$ galaxy cluster RXCJ0600–2007 with a magnification: $\mu = 29$ ($-7+4$).

GO-1567, PI: S. Fujimoto, in January 2023. The exposure time varies between bands, with 2491s for F356W and F444W, 1890s for F115W and F277W, and a deep integration of 4982s in F150W. ($\lambda_{\text{rest}} = 0.16, 0.21, 0.39, 0.50, \text{ and } 0.63 \mu\text{m}$)

PSF Matching to F444W and pixel size of $0.04''/\text{pixel} \rightarrow 0.2 \text{ kpc}/\text{pixel}$ at $z = 6.072$

RXCJ0600-z6-3 traces the entire galaxy. No lensing correction is applied on any images nor derived quantities, focusing mostly on the relative differences of the inferred properties when studying them in a resolved or an integrated approach.

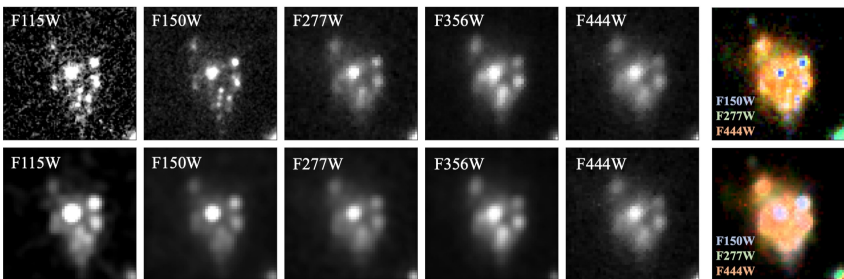


Fig. 1. Cutouts of the RXCJ0600-z6-3 image in all available NIRC*am* bands. The cutouts are 2 arcsec on a side and centered at $(\alpha, \delta) = (06:00:09.55, -20:08:11.26)$. The top row displays the observed images in their native resolution; the bottom row shows all images convolved with a kernel to match the F444W PSF. The right RGB three-colour images are constructed from the F150W (B), F277W (G) and F444W (R) bands with the scaling following the prescription from Lupton et al. (2004).

3. Methodology

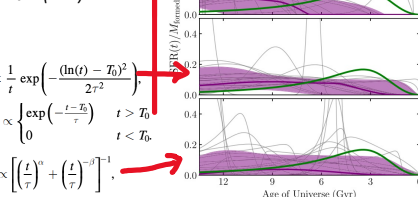
The SED modelling code *Bagpipes* (Carnall et al. 2018): BC03 + Kroupa (2001) IMF + Calzetti+00 attenuation curve. The metallicity centered at $0.1 Z_{\odot}$, with $\sigma = 0.2 Z_{\odot}$ (based on IFU)

Ionization parameter vary between $-3 < \log U < -1$, Cloudy *** Different types of the star formation history (SFH)

SFH model	Priors
Constant	Maximum age $\in [1 \text{ Myr}, 1 \text{ Gyr}]$
Log-normal	Age of the Universe at peak SF $\in [1 \text{ Myr}, 1 \text{ Gyr}]$ Full width at half maximum SF $\in [0, 1 \text{ Gyr}]$
Exponentially Declining	Time since SFH began $\in [1 \text{ Myr}, 1 \text{ Gyr}]$ Timescale of decrease $\tau \in [0, 10 \text{ Gyr}]$
Double-Power Law	Falling slope index $\in [0, 10]$ Rising slope index $\in [0, 10]$ Age of the Universe at turnover $\tau \in [1 \text{ Myr}, 1 \text{ Gyr}]$

Carnall+19 (right)

1. Exponentially Declining
2. Delay-tau
3. Log-normal
4. Double power law (DPL)



Segmentation and Pixel Selection: sklearn.cluster (exclude source)

S/N threshold per pixel is 1.9, 2.2, 3.5, 7.6, and 3.0 for the F115W, F150W, F277W, F356W, and F444W (Mean S/N for pixels with S/N > 1) \rightarrow 625 pixels



4. Results and Discussion

4.1. Spatially Resolved Analysis:

Centrally located clumps of young stars, surrounded by an extended region of older stellar populations Larger (~ 3) than the size of the F444W PSF (FWHM ~ 0.16)

Two very blue clumps in the UV slope map. A varying dust reddening surrounds the blue central clump.

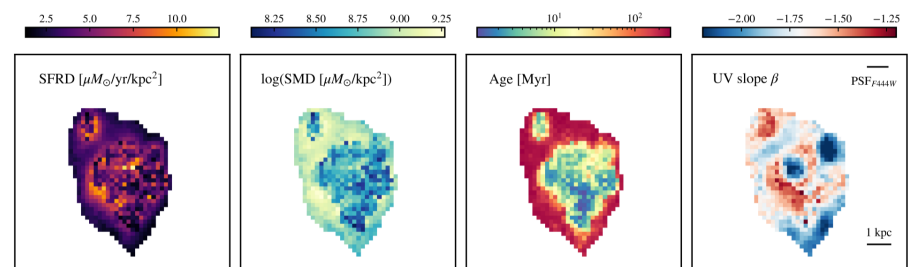


Fig. 2. Resulting physical properties for RXCJ0600-z6-3 inferred with *Bagpipes* using a constant SFH parameterisation. The maps are 2 arcsec per side and centered at $(\alpha, \delta) = (06:00:09.55, -20:08:11.26)$. From left to right, we display the star formation rate density, the stellar mass density, the inferred mass-weighted age of the stellar population, and the UV slope (β). The size of the F444W PSF (FWHM ~ 0.16) is also indicated on the top right.

4.2. The Integrated Field Spectrum from NIRS*pec*:

Table 1: The NIRS*pec* IFU equivalent widths are quite large, of $\geq 700 \text{ \AA}$ for $[\text{O III}] + \text{H}\beta$ and $\text{H}\alpha + [\text{N II}]$, typical at $z \sim 6$.

With the CSFH, a consistent value for EW($\text{H}\alpha + [\text{N II}]$), within the uncertainties; EW($[\text{O III}] + \text{H}\beta$) is larger than the IFU, although still in agreement within 2.5σ . Regarding the line fluxes, the photometric estimate is in good agreement.

Fig. 3: The NIRC*am* maps consistently reproduce the spatial distribution of the IFU measured lines, as well as their strength

A spatially-resolved analysis with only broad-band photometry, has the potential to provide a more complete picture of the internal structure and properties of galaxies.

4.3. The Spatial Resolution Effect on the Stellar Mass:

If having spatially-resolved observations affects the inferred physical parameters of a particular galaxy, when compared to spatially-integrated studies.

Resolved: the total stellar population is built up over extended timescales Integrated (except DPL): Younger, short, recent burst of star formation that dominates the light, but that has a lower total mass-to-light ratio Integrated (DPL): closest to the summed CSFH, with older stellar populations dominating the star formation activity over long timescales, and an inferred age of 130 Myr.

Table 2: The “mass offset”

The largest ΔM_r is given by SFH integrated runs (except DPL), with a significant offset of 0.5 dex, so that the resolved mass is more than 3 times larger than the unresolved one (outshining)

Table 2. Values for the stellar mass inferred in a spatially-integrated fit with *Bagpipes* using different star formation history parameterisations. The mass offset ΔM_r is calculated with respect to the resolved CSFH stellar mass of $\log(\mu M_r / M_{\odot}) = 10.2^{+0.1}_{-0.1}$, thus $\Delta M_r = \log(M_r^{\text{integrated}}) - \log(M_r^{\text{resolved}})$

SFH	$\log(\mu M_r / M_{\odot})$	ΔM_r [dex]
Constant	$9.7^{+0.4}_{-0.3}$	$0.5^{+0.2}_{-0.1}$
Exponentially declining	$9.7^{+0.3}_{-0.3}$	$0.5^{+0.1}_{-0.1}$
Log-normal	$9.7^{+0.3}_{-0.3}$	$0.5^{+0.1}_{-0.1}$
Double-Power Law	$10.4^{+0.4}_{-0.2}$	$-0.2^{+0.3}_{-0.2}$

4.4. The Ionizing Photon Production Efficiency (ξ_{ion}):

A representative galaxy (\approx sub- L^*) within the population that is thought to be the dominant during cosmic reionization.

Resolved ξ_{ion} : 25.53 ± 0.14 ; Integrated: 25.68 ± 0.08

5. Conclusion

RXCJ0600-z6-3, one of the multiple images of a highly-lensed galaxy at $z = 6.072$

The galaxy displays centrally-located clumps of young stellar populations embedded within extended regions of older stars.

The line fluxes inferred from NIRC*am* photometry with a CSFH can reproduce the spatial distribution and strength of the NIRS*pec* IFU emission line maps. Outshining, where young stars dominate the integrated light hiding underlying older stellar populations, affects the stellar mass values when comparing resolved and unresolved estimates. Resolving the galaxy yields ~ 0.15 dex lower ξ_{ion} , which could hint at spatially-integrated studies overestimating the contribution to reionization of targets similar to the one studied here.

Table 1. Values for the rest-frame equivalent widths and line fluxes (in cgs units of $\times 10^{-19} \text{ erg/s/cm}^2$) of $[\text{O III}] + \text{H}\beta$ and $\text{H}\alpha + [\text{N II}]$ inferred from the pixel-by-pixel modelling with *Bagpipes* on the NIRC*am* images, and calculated from the NIRS*pec* IFU measurements within a spatial aperture radius of 0.7 (S. Fujimoto et al. in prep.).

	NIRC <i>am</i>	NIRS <i>pec</i> /IFU
EW($[\text{O III}] + \text{H}\beta$) [\AA]	940 ± 20	711 ± 66
EW($\text{H}\alpha + [\text{N II}]$) [\AA]	596 ± 32	732 ± 125
$f_{[\text{O III}] + \text{H}\beta}$ [cgs]	2.8 ± 0.3	3.15 ± 0.02
$f_{\text{H}\alpha + [\text{N II}]}$ [cgs]	1.1 ± 0.2	1.44 ± 0.02

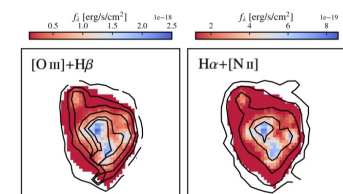


Fig. 3. Maps of the emission line fluxes obtained with the pixel-by-pixel SED fitting on the NIRC*am* images with a constant SFH. The contours correspond to the observed spectrum with the NIRS*pec* IFU (S. Fujimoto et al. in prep.).

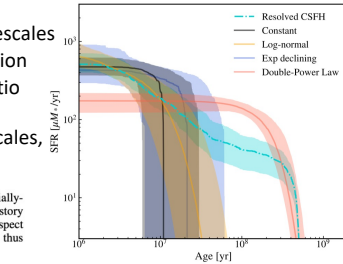


Fig. 4. Star formation history of the resolved constant SFH analysis (turquoise dash-dotted curve), compared with the resulting SFH of the spatially-integrated fits obtained by varying the SFH form. The shaded areas correspond to the 16–84th percentile range in each case.

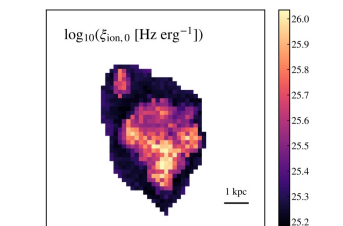


Fig. 7. Inferred 2D distribution of the ionizing photon production rate $\log_{10}(\xi_{\text{ion},0} [\text{Hz erg}^{-1}])$, derived using Equation 1.